Bilinear softening parameters and equivalent LEFM R-curve in quasibrittle failure

S. Morel , C. Lespine , J.-L. Coureau , J. Planas , N. Dourado

Université Bordeaux 1, US2B (UMR 5103), 351 cours de la Libération, 33405 Talence cedex, France
Departamento de Ciencia de Materiales, ETS de Ingenieros de Caminos, UPM Profesor Aranguren s/n 28040 Madrid, Spain
CITAB/UTAD, Departamento de Engenharias, Quinta de Prados, 5000-911 Vila Real, Portugal

A B S T R A C T

For composites and adhesive joints, the determination of the cohesive zone parameters from Double Cantilever Beam specimens loaded with pure moments is now well established and documented. However, for quasibrittle materials used in Civil Engineering such as concrete or wood, the difficulty to apply a pure bending moment lies inappropriated the method used for composites. Nevertheless, the one-to-one correspondence which exists between the R-curve and the softening curve is here revisited and adapted for any kind of specimen geometry and for the bilinear approximation of the softening function, well-known to successfully describe the failure of a wide group of quasibrittle materials. It is shown that even though the connections between the cohesive parameters and the 'equivalent LEFM' R-curve are geometry and material dependent, their trends are preserved whatever the specimen geometry and the material are. The outline of a general estimation procedure of the cohesive zone parameters funded on the equivalent LEFM R-curve is proposed.

Keywords:
Quasibrittle fracture
R-curve
Cohesive zone model
Bilinear softening function
Energy distribution
Critical opening
Plateau value of the resistance
Cohesive fracture energy

1. Introduction

Fracture of quasibrittle materials and especially those used in Civil Engineering such as concretes and mortars (especially high strength concretes), various rocks, wood and wood particle board, is characterized by the existence of a large *fracture process zone* (FPZ) which develops ahead of the crack tip. In this FPZ, various toughening mechanisms are mobilized such as microcracking, crack branching, or crack bridging. Hence, nonlinear fracture theories are required to describe the fracture behavior of quasibrittle materials. Conceptually, the simplest and the most efficient model to characterize the quasibrittle failure is the cohesive zone model (see Elices et al., 2002; Bažant, 2002; Planas et al., 2003, for recent reviews). Thus, it is nowadays firmly established that the accurate description of the quasibrittle failure of concrete, rocks and wood, needs to use a concave softening behavior or its bilinear approximation which also allows describing the quasibrittle failure with reasonable accuracy.

On the other hand, if the determination of the cohesive zone parameters based on experimental tests performed on Double Cantilever Beam (DCB) specimens loaded with pure moments is now well established and documented especially for composites or adhesive joints (Suo et al., 1992; Lindhagen and Berglund, 2000; Sørensen and Jacobsen, 2003), such a method is not easily applicable for quasibrittle materials used in Civil Engineering because of the difficulty to apply a pure bending moment without inducing brittle failures on these materials and/or the consequent self-weight effect of specimens (due to the large specimen dimension required to avoid FPZ confinement) which turns difficult sophisticated loading setup. For instance, the fracture tests of concrete and rocks are usually performed from Single Edge Notched Beams (SENB) loaded in three-point or four-point bending (Bažant, 2002; Planas et al., 2003). These specimen geometries and the loading setup limit the tensile zones in the specimen and so the inherent brittle failures. In the case of wood, if the choice of the specimen geometry is more important (DCB, TDCB where T designates the term tapered and SENB are the specimen geometries usually used), the nonlinear relationship between applied load and displacement (or applied moment and rotation) due to the large indentation displacements at the loading points turns difficult the use of the procedure proposed for composites and adhesive joints. Moreover, as for concrete, the use of large specimen dimensions induces a nonnegligible self-weight effect of specimen which turns also difficult sophisticated loading setup. Thus, despite the success of cohesive zone models, the determination of the cohesive parameters from experimental load-displacement curves (or load–COD curves) obtained for concrete and wood is still a long and tiresome operation (Wang, 2006; Dourado et al., 2008). However, if the estimate of cohesive parameters from DCB specimens loaded with pure moments cannot easily be applied for concrete and wood, the one-to-one correspondence which exists between the R-curve and the softening curve previously studied by Suo et al. (1992) is here revisited and adapted for any kind of specimen

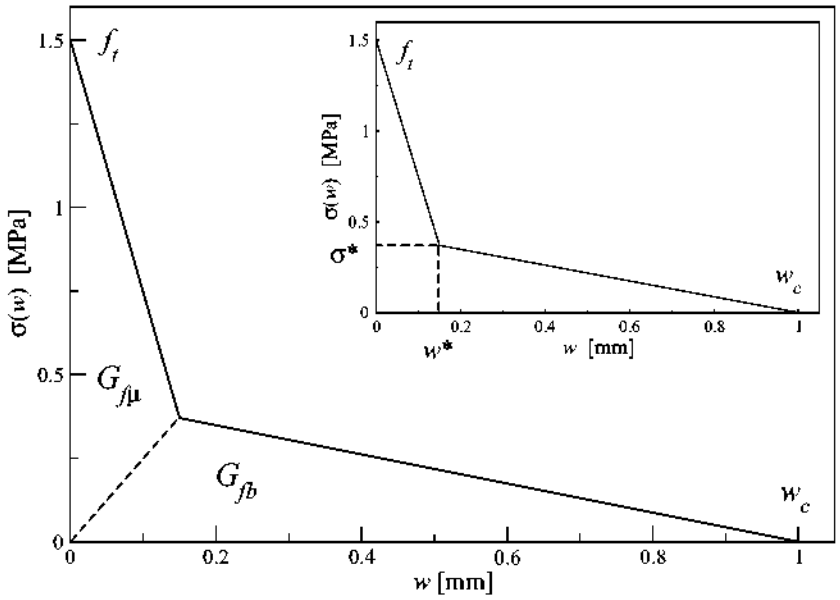

Fig. 1. Bilinear softening diagram used in the cohesive zone model. The cohesive fracture energy G_f (area under the stress-opening displacement curve) corresponds to the sum of the arbitrarily defined energies $G_{f\mu}$ and G_{fb} which can be conceptually related to the microcraking and the crackbridging phenomena respectively.

geometry (and any kind of loading) and especially for an R-curve expressed as a function of the equivalent linear elastic crack length which is usually the case of quasibrittle materials used in Civil Engineering. Thus, for various specimen geometries (DCB, TDCB and SENB), the connections between the bilinear softening properties and the equivalent LEFM R-curve are studied and the outline of a general estimation procedure of the cohesive zone parameters is proposed.

2. Cohesive zone model

The basic hypothesis of cohesive zone models is that, for mode I failure, the FPZ can be described through a fictitious line crack (which is usually characterized by a zero thickness interface) which transmits normal stresses σ. The magnitude of these stresses is a function (monotonically decreasing) of the opening displacement w of the interface: $\sigma = f(w)$ which is called the softening function (Hillerborg et al., 1976; Petersson, 1981; Guinea, 1995). An example can be seen in Fig. 1.

The cohesive zone initiates when the normal stress σ reaches the tensile strength f_t, then, the cohesive zone opens while transferring normal stresses from one face to the other. The normal stress in the cohesive zone decreases with respect to the opening w and becomes zero at some critical opening w_c, i.e., $\sigma = f(w_c) = 0$. The area under the entire stress-opening curve $f(w)$ is usually called the cohesive fracture energy G_f [J/m^2], i.e. the total energy required to completely separate the interface at a given point and expressed per unit area of the crack plane.

It is now firmly established that the quasibrittle failure of concrete, rocks or wood needs to use a concave softening which can be described from exponential or polynomial functions (Elices et al., 2002; Bažant, 2002; Planas et al., 2003). Nevertheless, the bilinear approximation[1] of the concave softening proposed by Petersson (1981) and plotted in Fig. 1 allows describing, with reasonable accuracy, the fracture of materials as different as concretes and mortars (Elices et al., 2002; Bažant, 2002; Planas et al., 2003), ceramics (Dasgupta et al., 1998) or wood (Boström, 1994; Lespine, 2007; Dourado et al., 2008). In the literature, there exist various manners to define the cohesive zone parameters of the bilinear softening function. In the present study, we propose to determine the shape of the cohesive function by:

- (i) the cohesive fracture energy G_f[J/m^2],
- (ii) the energy distribution between the two cohesive energies $G_{f\mu}$ and G_{fb} as shown in Fig. 1 defined from the ratio $G_{f\mu}/G_f$,
- (iii) the critical opening w_c [mm],
- (iiii) the tensile strength f_t [MPa].

As shown in Fig. 1, the sum of the energies $G_{f\mu}$ and G_{fb} corresponds to the cohesive energy G_f, i.e. $G_f = G_{f\mu} + G_{fb}$. Although there is no direct quantitative evidence, it is widely accepted that the initial steep descent of the softening curve is governed by localized microcracking, while the mild softening of the tail is governed by crack bridging mecanisms; in this sense $G_{f\mu}$ and G_{fb} can be interpreted, schematically, as the energies related to the microcracking and the crack bridging cohesive behaviors, respectively, although the partition is obviously not unique, and must be understood just as a convenient conceptual simplification. Note that the decomposition of the fracture energy G_f through two components $G_{f\mu}$ and G_{fb} avoids to consider the coordinates (w^*, σ^*) of the crossover point between the two straight lines in Fig. 1 to the benefit of a single undimensional parameter $G_{f\mu}/G_f$ corresponding to the distribution of the cohesive energy between the microcracking phenomenon and the crack bridging one.[2] Finally, if a smooth softening function (obtained from exponential or polynomial functions) leads usually to a better fit of experimental data compared to the bilinear approximation (Fig. 1), it is difficult to drive accurately the cohesive energy distribution from a smooth function.

3. Connections between cohesive zone parameters and R-curve

The connections between the cohesive zone properties G_f, $G_{f\mu}/G_f$, w_c and f_t and the R-curve are studied from cohesive zone

[1] Fig. 1 corresponds only to the softening behavior, i.e., the initial elastic part and especially the initial stiffness of the interface are not represented.

[2] From the proposed definition of both cohesive energies $G_{f\mu}$ and G_{fb}, the coordinates of the crossover point between the two straight lines in Fig. 1 are given by: $w^* = 2G_{f\mu}/f_t$ and $\sigma^* = 2G_{fb}/w_c$.

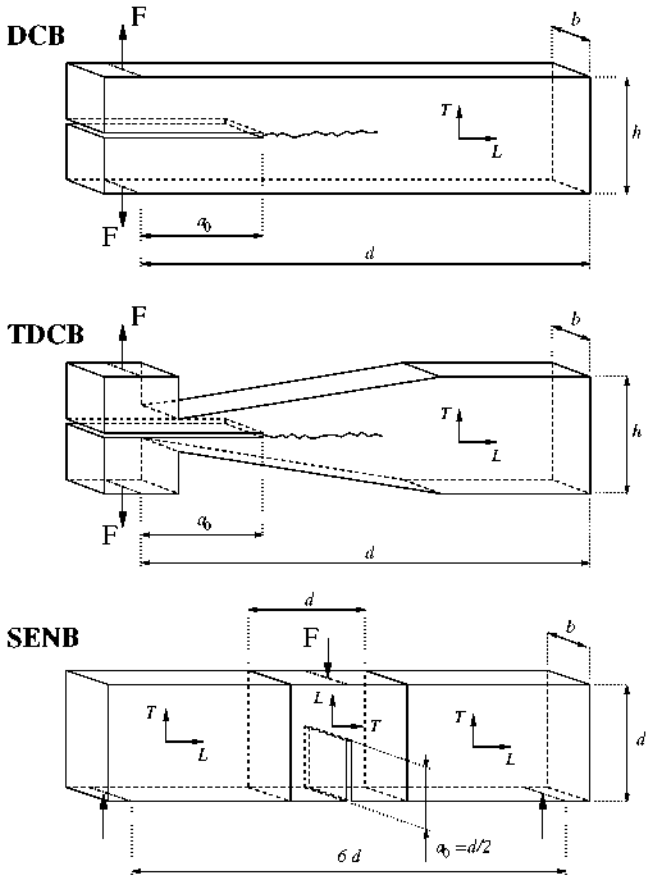

Fig. 2. Geometries of the three fracture specimens (DCB, TDCB and SENB) used for cohesive zone simulations.

simulations performed on three different specimen geometries: DCB, TDCB and SENB fracture specimens (Fig. 2) constituted by an orthotropic material.

In this section, for clarity reasons, the connections will only be illustrated for the DCB specimen (Fig. 2), the results obtained from TDCB and SENB specimens being analogous to those obtained for the DCB geometry. Note that, as previously mentioned, the DCB and TDCB specimens are loaded with forces and not pure moments.

3.1. Cohesive fracture energy and plateau value of the R-curve

The first step consists in studying the general connection between a given softening curve and the load–displacement and corresponding equivalent LEFM R-curve responses from an accurate observation of the cohesive fracture process obtained from numerical simulations.

A numerical simulation is performed from the DCB specimen (Fig. 2) with $h = 70$ mm, $b = 20$ mm, $a_0 = 90$ mm and $d = 350$ mm and for a set of cohesive zone parameters selected to be representative of wood (Norway spruce, *Picea abies L.*) as described in (Lespine, 2007; Dourado et al., 2008): $G_f = 286$ J/m^2, $w_c = 1.0$ mm, $G_{f\mu}/G_f = G_{fb}/G_f = 50\%$ and $f_t = 1.0$ MPa. The elastic properties of wood are $E_L = 8900$ MPa, $E_T = 410$ MPa, $\nu_{LT} = 0.44$ and $G_{LT} = 410$ MPa where L and T correspond to the longitudinal and tangential wood directions respectively as shown in Fig. 2. The load–displacement curve obtained under displacement control is plotted in Fig. 3(a).

Within the framework of 'equivalent Linear Elastic Fracture Mechanics' (Bažant, 2002; Elices and Planas, 1993; Planas et al., 1993; Fett et al., 2000; Ferreira et al., 2002; Morel et al., 2003, 2005), the increase of the specimen compliance observed on the load–displacement curve plotted in Fig. 3(a) can be attributed to the propagation of an equivalent LEFM crack (i.e., a sharp traction-free crack which gives, according to LEFM, the same secant compliance as the actual crack with its cohesive zone). On this basis, the energy stored in the structure, characterized by the complementary energy W^*, can be expressed as a function of the elastically equivalent crack length a: $W^*(a) = P^2\lambda(a)/2$, where P is the load applied to the specimen and $\lambda(a)$ the specimen elastic compliance for an equivalent crack length a. Thus, given the compliance function $\lambda(a)$ which can be computed, for example, from a finite element analysis or taken from closed form formulas available in the literature, the determination of the R-curve follows basically three steps: (1) for a point on the experimental curve, say point 1, the secant compliance λ_1^{exp} is determined corresponding to an experimental load P_1^{exp}; (2) the corresponding equivalent crack extension a_1 is determined by solving the equation $\lambda(a_1) = \lambda_1^{exp}$ for a_1; (3) the energy release rate, which in static crack growth must coincide with the crack growth resistance G_R, is then determined from the expression:

$$G(a_1) = G_R(a_1) = \frac{1}{b}\frac{\partial W^*(a)}{\partial a}\bigg|_{a=a_1} \equiv \frac{P_1^2}{2b}\frac{d\lambda(a)}{da}\bigg|_{a=a_1} \tag{1}$$

where b is the thickness of the specimen (Fig. 2).

The resistance curve or R-curve represented in Fig. 3(b) has been obtained from the load–displacement curve plotted in Fig. 3(a) using Eq. (1). The initial rising part of the curve shows a strong dependence on the equivalent LEFM crack length a or, more specifically, on the equivalent crack extension $\Delta a = a - a_0$. The figure also shows that after the rising part, a plateau is reached for a crack extension denoted as Δa_c, after which the crak growth resistance remains constant and equal to a plateau value denoted here as G_{Rc}, i.e. $G_R(a \geqslant a_c) = const. = G_{Rc}$.

In order to illustrate the part of the load–displacement response corresponding to the plateau of the R-curve, the theoretical LEFM load–displacement curve obtained for a constant value of the resistance to crack growth $G(a) = G_{Rc}$ is plotted in Fig. 3(a) (dotted curve) and denoted as *LEFM curve*. It can be seen that for a crack length $a \geqslant a_c$, the load–displacement curve is superimposed onto the LEFM curve emphasizing the part of the $P - \delta$ response related to the propagation at constant resistance G_{Rc}. Thus, the existence of a plateau in the resistance curve suggests that the cohesive zone reaches a steady state when the equivalent crack extension reaches the critical value $\Delta a_c = a_c - a_0$, and thereafter propagates in a self-similar steady way.

The existence of a steady state regime is a well-known result mentioned in numerous works (see, for instance, Suo et al., 1992; Lindhagen and Berglund, 2000; Sørensen, 2002; Sørensen and Jacobsen, 2003; Coureau et al., 2006; Lespine, 2007). The main consequence of the steady state regime is the equality between the value of the crack growth resistance G_{Rc} at the plateau and the value of the cohesive fracture energy G_f, as turns out to be the case in the present analysis, since $G_{Rc} = G_f = 286$ J/m^2, as can be observed in Fig. 3(b). As a matter of fact, three well-known conditions allow to define the steady state propagation an hence the equality $G_{Rc} = G_f$.

First, steady-state propagation requires that the length of the cohesive zone l_{coh} remains constant along the plateau of the R-curve as shown in Fig. 3(b). The length of the cohesive zone is defined as the distance (along the potential crack path) between the tip of the stress-free crack[3] and the point where the

[3] Operatively defined as the length a_{sf}, along the potential crack path, between the axis of the applied load and the first two nodes of the interface at which the normal stress is not zero.

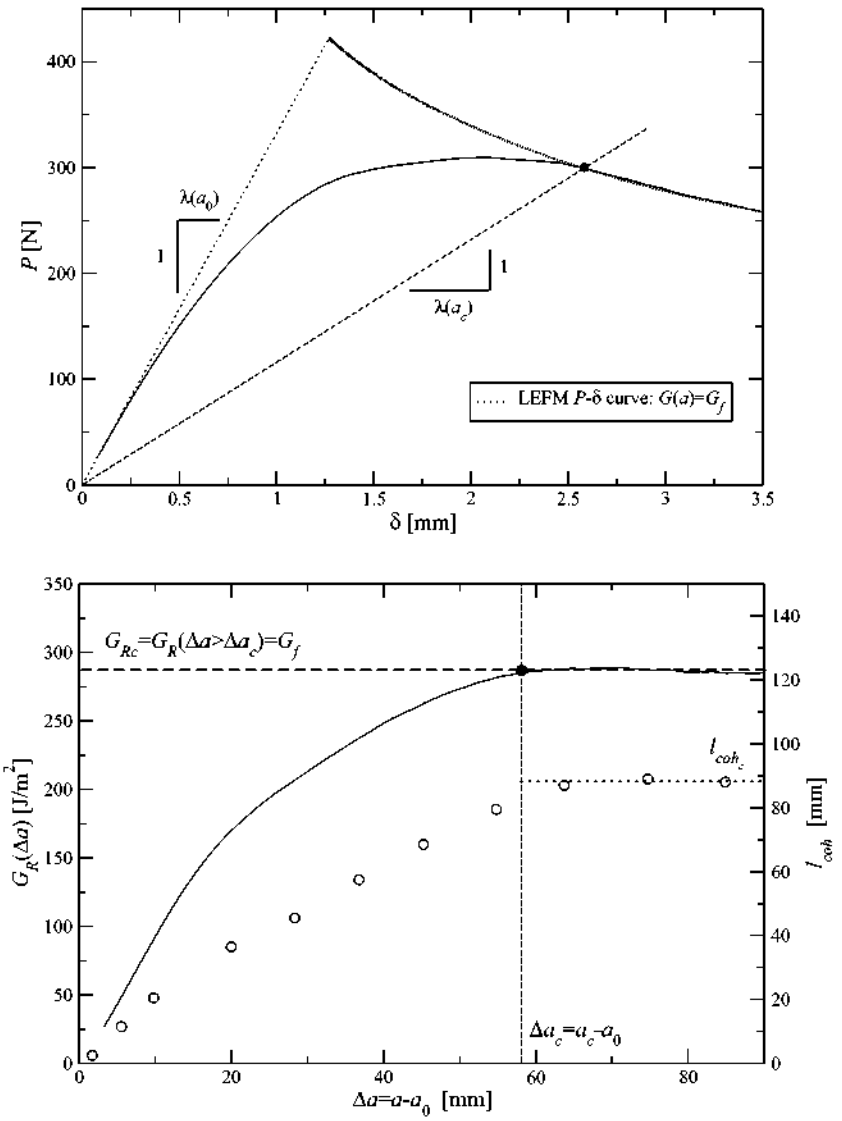

Fig. 3. Numerical load–displacement curve (a) and its corresponding R-curve (b) obtained for a set of cohesive zone parameters selected to be representative of a wood specie (Norway spruce, *Picea abies L.*) as described in Lespine (2007) and Dourado et al. (2008): $G_f = 286\ \mathrm{J/m^2}$, $w_c = 1.0$ mm, $G_{fII}/G_f = G_{fb}/G_f = 50\%$ and $f_t = 1.0$ MPa. The plateau value of the R-curve G_{Rc} corresponds to the cohesive fracture energy G_f, i.e. $G_{Rc} = G_f$.

normal stress is equal to the tensile strength f_t. It can be seen in Fig. 3(b) that the cohesive zone increases initially with increasing equivalent crack extension Δa until it reaches a plateau value, noted as l_{cohc}, for an equivalent crack extension numerically indistinguishable from Δa_c. Moreover, during the increase in length of the cohesive zone (i.e., for $\Delta a < \Delta a_c$), the length of the stress free crack a_{sf} coincides to the one of the initial notch a_0 (i.e., $a_{sf} = a_0$) while, for crack length increments $\Delta a \geqslant \Delta a_c$, the stress-free crack propagates, i.e., $a_{sf} > a_0$.

Second, steady state propagation requires that the cohesive stress distribution over the cohesive zone remains constant during its propagation as shown in Fig. 4. Indeed, as shown from four normal stress profiles along the cohesive interface $\sigma(r)$ (where r denotes the abscissa along the cohesive zone considered from the tip of the stress free crack) corresponding to four different lengths a_sf of the stress free crack, the cohesive stress profiles are nearly indistinguishable.

And third, if we face a translational steady state, the location of the equivalent elastic crack tip relative to the cohesive zone should be constant along the plateau. Fig. 5 shows the evolution of the position of the tip of the equivalent elastic crack relative to the stress-free crak tip, $a - a_{sf}$, versus the equivalent crack increment Δa. Consistently with previous considerations, $a - a_{sf}$ evolves along a 1:1 line up to the initiation of the energy plateau (because $a_{sf} = a_0$ for $a \leqslant a_c$), and then remains approximately constant, thus confirming a true steady state. Note that $a - a_{sf}$ is smaller than the size of the cohesive zone, so that the equivalent elastic crack tip always lies within the cohesive zone. Moreover, in the plateau, when the stress-free crack extends by da, the equivalent elastic crack extends by the same amount.

Consistently with the foregoing observations, the development of the cohesive zone can be sketched as shown in Fig. 6. As a consequence of the properties just analyzed, when the crack reaches the steady-state, the propagation by da of the stress-free crack with its critical cohesive zone is expected to require the energy $dW = G_f(bda)$ where G_f corresponds to the energy required to separate completely the crack faces at a given point and (bda) corresponds to the cracked surface during the increment da. Moreover, since an advance by da of the stress-free crack corresponds to the same advance in terms of equivalent LEFM crack, the macroscopic resistance to crack growth can be estimated from the elastic energy released dW as:

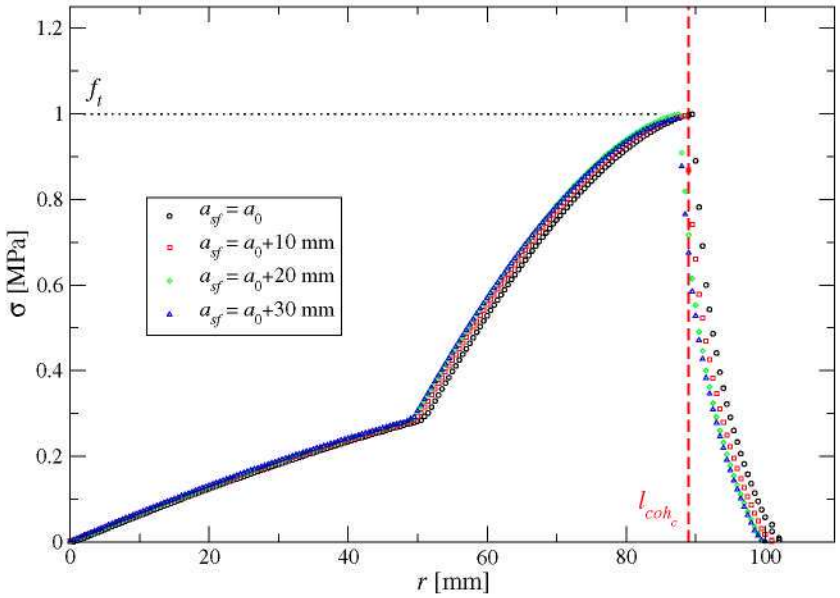

Fig. 4. Normal stress profiles $\sigma(r)$, where r denotes the abscissa along the cohesive interface considered from the tip of the stress-free crack, observed for several lengths of the stress-free crack, i.e., $a_{sf} \geqslant a_0$ (or in other terms, for several equivalent crack lengths $a \geqslant a_c$).

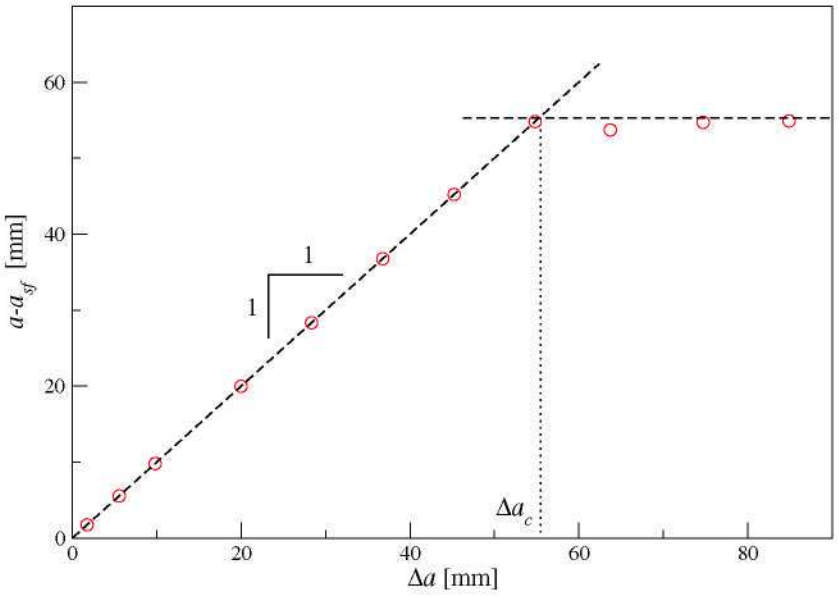

Fig. 5. Comparison between the length of the stress-free crack a_{sf} and the equivalent crack length a.

$$G_R(a \geqslant a_c) = \frac{dW}{bda} = G_f = const. = G_{Rc}. \tag{2}$$

which defines a plateau value of the resistance as expected.

Thus, as shown from Figs. 3(b), 4, 5, a true steady state regime is here obtained in the case of a DCB specimen loaded with forces and not with pure bending moments as suggested by Suo et al. (1992). Indeed, Suo et al. (1992) has shown that a DCB specimen loaded with forces only leads to a steady state propagation if the ratio $(a_0 + l_{cohc})/h$ is sufficiently large while the ratio l_{cohc}/h is small. In the present case, if the first condition is achieved, the second one (i.e., a small l_{cohc}/h) is not respected and yet a steady state propagation is observed. This disagreement between the Suo's recommendations and the results observed here is doubtless due to the fact the cohesive function used by Suo (a rigid plastic one (Suo et al., 1992)) is very different from the bilinear one used here. As a matter of fact, whatever the specimen geometry and the loading conditions are, a steady state propagation will be observed if the stress free crack and its critical cohesive zone might propagate freely, i.e., without confinement of the cohesive zone during the propagation (see Dourado et al. (2008) for more details). In this sense, a DCB specimen will be preferable to a SENB one because, for the same specimen dimension, the ligament is longer in DCB than in SENB. Thus, if a steady state regime has also been observed in the TDCB specimen (Fig. 2) for the same set of cohesive parameters and the same specimen size as those used for the DCB specimen, the observation of a steady state regime in the SENB specimen of analogous size has required a different set of cohesive parameters with especially smaller w_c and G_f.

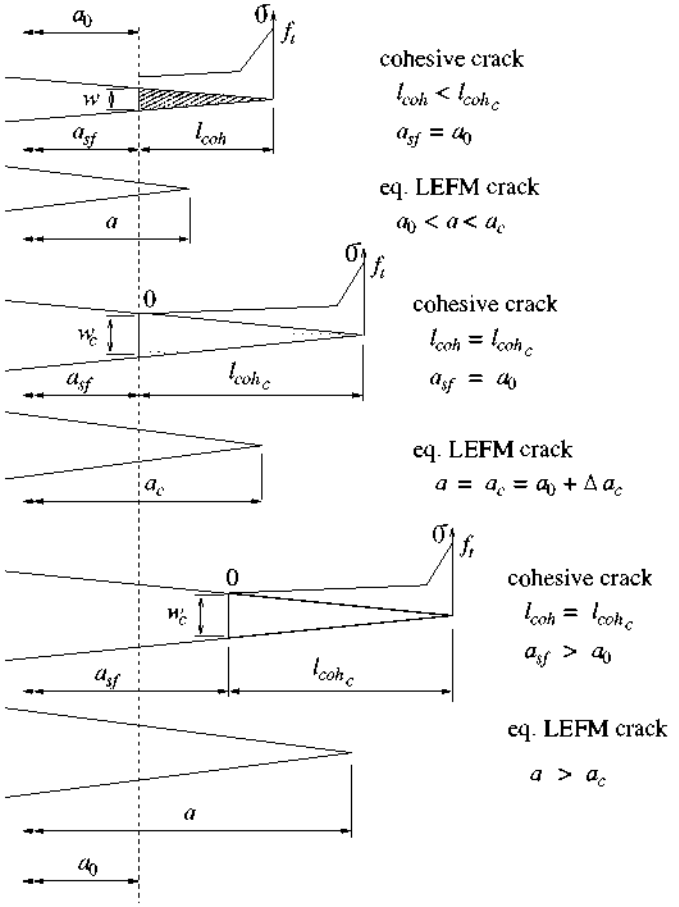

Fig. 6. Sketch of the cohesive zone behavior: comparison of the stress-free crack length a_{sf} with the equivalent LEFM crack length a for different stages of crack propagation.

On the other hand, in quasibrittle materials such as concrete, the cohesive fracture energy G_f is usually estimated from the mean fracture energy G_F which is defined as the total work of fracture (measured as the area under the load–displacement curve) divided by the total cracked area instead of the plateau value of the R-curve G_{Rc}. However, as usually performed for composites materials (Lindhagen and Berglund, 2000; Sørensen and Jacobsen, 2003) or adhesive joints (Sørensen, 2002), the use of the plateau value G_{Rc} of the R-curve is preferable in order to estimate the cohesive fracture energy G_f because the accurate measurement of the fracture energy G_F requires to fracture completely the specimen and since the load–displacement curve gets usually a long tail (where the curve asymptotically approaches the horizontal axis) then it turns difficult the accurate measurement of the area.[4]

3.2. Influence of the critical opening w_c

To ascertain the influence of the critical crack opening on the fracture process, numerical tests were carried out for different values of the critical opening w_c while the cohesive fracture energy G_f, the energy distribution (characterized by the ratio $G_{f\mu}/G_f$) and the tensile strength f_t were kept constant ($G_f = 286\,\mathrm{J/m^2}$, $G_{f\mu}/G_f = 50\%$, $f_t = 1.0$ MPa, while $w_c = 0.8$, 1.0, 1.2 and 1.6 mm. The resulting load–displacement curves for the DCB specimen are plotted in Fig. 7(a) and the corresponding R-curves, determined from Eq. (1), are plotted in Fig. 7(b).

It can be seen in Fig. 7(a) that the increase in the critical opening w_c influences the location of the junction point between the load–displacement curve and the theoretical LEFM one (i.e. the curve obtained according to Eq. (1) for $G(a) = G_{RC} = G_f$). As previously mentioned, this junction point is reached when the opening displacement w at the tip of the initial notch is equal to the critical opening w_c which corresponds to the onset of the steady state propagation. In terms of resistance curve, this point corresponds to the onset of the plateau, i.e. $G_R(\Delta a_c) = G_{Rc}$ as shown in Fig. 7(b).

Both Fig. 7(a) and (b) clearly shows that the critical crack extension $\Delta a_c = a_c - a_0$ increases with increasing w_c. The evolution of Δa_c with w_c is plotted in Fig. 8, together with the evolution of the critical cohesive zone length l_{cohc}. It can be seen that the curves for Δa_c and l_{cohc} vs w_c run nearly parallel. A closer examination shows that the relation between Δa_c and l_{cohc} is linear with a correlation coefficient of 0.998 and that:

$$\Delta a_c = 0.887^{\pm 0.039}(l_{cohc} - 22.3^{\pm 5.3}) \tag{3}$$

Further studies shown in the sequel show that the critical crack opening is the dominant parameter influencing the size of the critical equivalent crack extension and the critical size of the cohesive zone, which is in agreement with previous findings by Planas and Elices (1993) for the asymptotic behavior of the cohesive crack for infinitely large specimens.

Similar results are obtained in the simulations carried out for TCDB and SENB specimens, which indicates that the dominant effect of the critical crack opening on the critical equivalent crack extension and on the critical size of the cohesive zone is valid for a variety of specimen geometries.

3.3. Influence of the cohesive energy distribution

In this section, the influence of the energy distribution is studied in considering several ratios $G_{f\mu}/G_f = 35$, 50, and 65% while, the cohesive fracture energy G_f, the tensile strength f_t and the critical opening w_c are kept constant ($G_f = 286\,\mathrm{J/m^2}$, $f_t = 1.0$ MPa and $w_c = 1.0$ mm). The load–displacement curves and the corresponding R-curves obtained from the DCB specimen for the various energy distributions are plotted in Fig. 9(a) and (b), respectively. The first important result is that, for a constant critical opening w_c and despite the different energy distributions, all the load–displacement curves join in the same point in Fig. 9(a) and hence lead to an identical equivalent LEFM length Δa_c of the cohesive zone as shown in Fig. 9(b). On the other hand, it can be seen in Fig. 9(a) that the energy distribution influences significantly the intermediate part of the load–displacement curve around the peak load and especially the maximum load itself. A similar effect is observed for the R-curve as shown in Fig. 9(b) which clearly shows that the distribution of energy affects only the intermediate portion of the rising part of the R-curve while leaving unchanged both the starting part and the plateau.

The critical length of the cohesive zone l_{cohc} and the critical equivalent crack extension Δa_c were determined from the numerical results, and have been plotted in Fig. 10, which clearly show that these variables are not influenced by the energy distribution.

Similar results are obtained in the simulations carried out for TCDB and SENB specimens, which indicates that the cohesive energy distribution, which characterizes the shape of the softening function, does not influence the response when the plateau is reached, but plays a crucial role over the central half of the raising part of the R-curve (i.e., for $0.25\Delta a_c \lesssim \Delta a \lesssim 0.75\Delta a_c$). Thus, the energy distribution determines the macroscopic mechanical response and especially the magnitude of the peak load as previously

[4] On purely theoretical grounds, the cohesive fracture energy, the plateau resistance and the fracture energy are all equal: $G_f = G_{Rc} = G_F$.

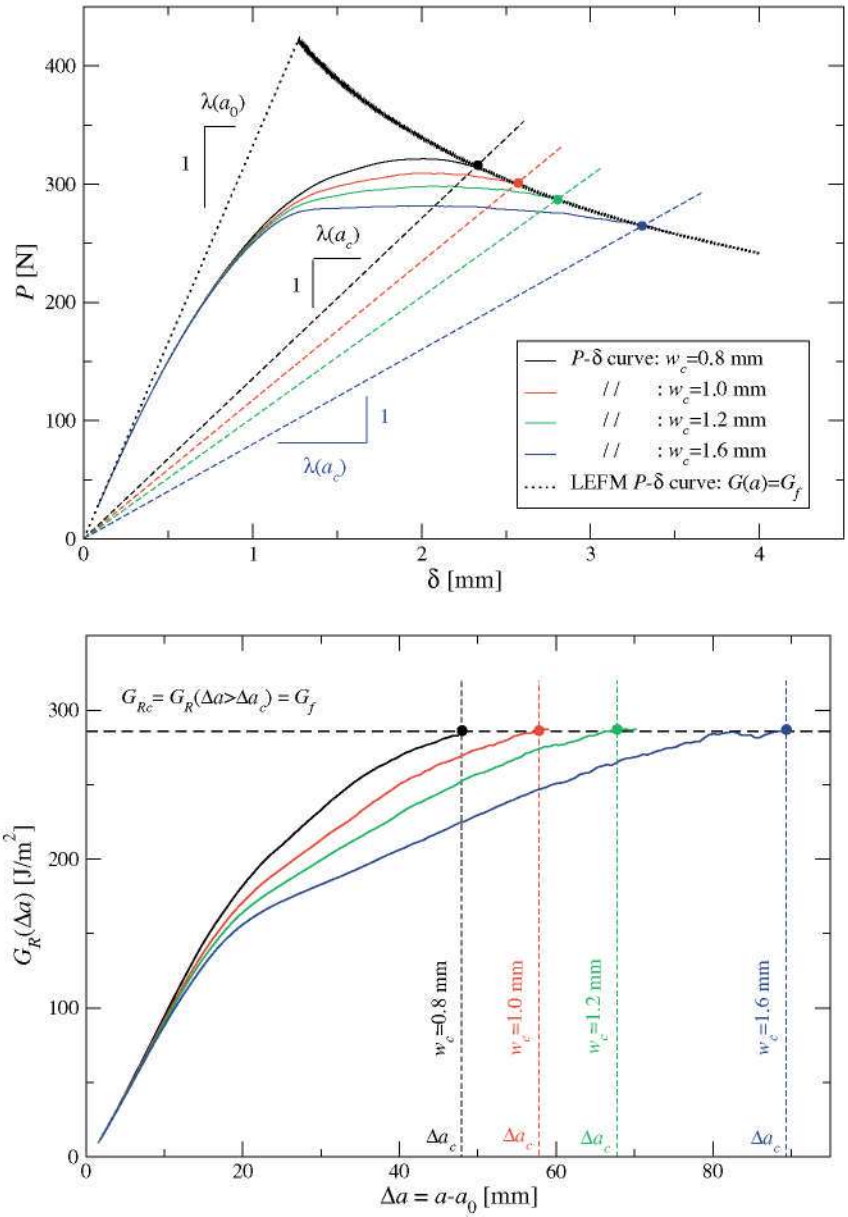

Fig. 7. Load–displacement curves (a) and their corresponding R-curves (b) obtained in the case of different values of the critical opening $w_c = 0.8,\ 1.0,\ 1.2$ and 1.6 mm while the energy distribution is kept constant $G_{f\mu}/G_f = G_{fb}/G_f = 50\%$ as well as the tensile strength $f_t = 1.0$ MPa and the cohesive fracture energy $G_f = G_{Rc} = 286\,\mathrm{J/m^2}$.

observed by many researchers, with different parametrizations of the softening curve, starting for concrete, in the middle eighties, and restated many times since then until recently, as for example in Chandra et al. (2002).

On the other hand, from a different parametrization of the bilinear softening curve for concrete, Park et al. (2008) have proposed that the crossover point of the crack opening width (noted as w^* in Fig. 1) is the same as the critical crack tip opening displacement ($CTOD_c$). However, if this proposition is in agreement with the behavior observed from an SENB specimen geometry, this is not the case for other geometries such as DCB or TDCB. Indeed, for DCB and TDCB specimens the crossover point of the crack opening is obtained before the peak load (i.e., in the pre-peak regime as shown by Lespine, 2007).

3.4. Influence of the tensile strength f_t

In this section, different values of the tensile strength f_t are tested ($f_t = 0.8,\ 1.0,\ 1.3$ and 1.6 MPa) while the cohesive fracture energy G_f, the energy distribution and the critical opening w_c are kept constant (i.e., $G_f = 286\,\mathrm{J/m^2}$, $G_{f\mu}/G_f = 50\%$ and $w_c = 1.0$ mm). The load–displacement curves obtained from the DCB specimen are plotted in Fig. 11(a) while their corresponding R-curves are plotted in Fig. 11(b).

It can be seen in Fig. 11(a) that, for fixed values of the critical opening w_c and of the energy distribution $G_{f\mu}/G_f$, the tensile strength f_t mainly influences the part of the load–displacement curve related to the onset of the equivalent LEFM crack propagation, i.e. the initial part of the nonlinear response, which, for a sharp notch, starts from the very beginning of the loading because of the stress singularity at the notch tip; for a nonsharpened notch, a threshold exists since there is no stress singularity, and the cohesive crack starts to grow only after the stress at the notch root reaches the tensile strength f_t.

In any case, at the beginning of crack growth, the crack opening is very small all over the fracture zone, which means that the cohesive stress is nearly constant and close to f_t all over the (small) cohesive zone. This means that the initial deviation from linearity

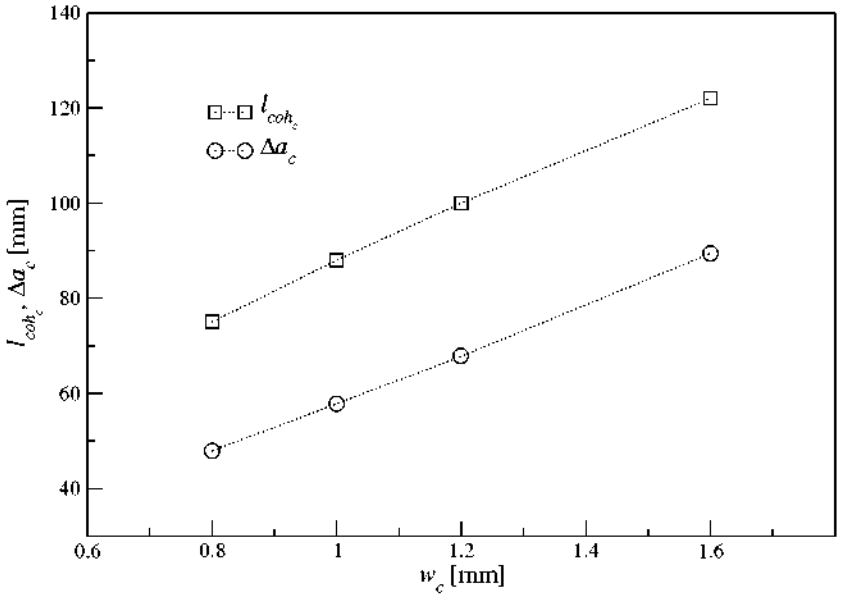

Fig. 8. Evolutions of the critical length of the cohesive zone l_{coh_c} and of the critical crack length extension $\Delta a_c = a_c - a_0$ with respect to the critical opening $w_c (0.8 \leqslant w_c \leqslant 1.6$ mm).

in the load–displacement curve must be totally controlled by the tensile strength f_t and, effectively, it can be seen in Fig. 11(a) that the initial deviation from linearity is larger the smaller the tensile strength. The dominant influence of f_t on the response at the beginning of loading is also observable on the corresponding R-curve (Fig. 11b); however, the influence of the tensile strength is strong only roughly on the first-quarter of the rising part of the R-curve. In the middle part, the influence of the cohesive energy distribution is stronger (as shown in Section 3.3).

As in previous sections, the critical length of the cohesive zone l_{coh_c} and its equivalent crack extension Δa_c were determined and plotted in Fig. 12 versus the tensile strength f_t. The critical length of the cohesive l_{coh_c} slightly decreases with increasing f_t while the equivalent crack extension Δa_c remains essentially constant.

The influence of the tensile strength f_t on the TDCB and SENB specimens is analogous to the one observed for the DCB geometry in all respects.

4. Discussion

4.1. Dependence of Δa_c on softening parameters and specimen size

According to the results presented in Sections 3.2, 3.3 and 3.4, Δa_c is essentially controlled by the critical crack opening w_c, for a given specimen size. To ascertain the general dependence of Δa_c on softening parameters and specimen size, we use the fact that it can be shown from dimensional analysis and the equations of the cohesive crack – see, e.g., Elices and Planas (1993) – that the critical equivalent crack extension must depend on the size of the specimen and on the cohesive crack parameters in the form:

$$\frac{\Delta a_c}{\ell_{ch}} = \phi_1\left(\frac{D}{\ell_{ch}}, \frac{w_c}{w_{ch}}, \frac{G_{f\mu}}{G_f}\right) \tag{4}$$

in which $\phi_1(\cdot)$ is a dimensionless function, D is a characteristic dimension of the specimen (beam depth, for example, all the remaining in-plane dimensions being proportional to it), and Hillerborg's characteristic length ℓ_{ch} and the characteristic crack opening w_{ch} are defined as:

$$\ell_{ch} = \frac{E^\star G_f}{f_t^2} \quad w_{ch} = \frac{G_f}{f_t}, \tag{5}$$

where $E^\star$ is the effective Young modulus.[5] Now, from the results in Section 3.3, it turns out that, over the range studied, Δa_c does not depend on $G_{f\mu}/G_f$ when the remaining parameters are kept constant, which implies that $\phi_1(\cdot)$ neither depends on $G_{f\mu}/G_f$. So, we can rewrite the foregoing equation as:

$$\frac{\Delta a_c}{\ell_{ch}} = \phi_2\left(\frac{D}{\ell_{ch}}, \frac{w_c^2}{w_{ch}^2}\right) \tag{6}$$

Now, from the results in Section 3.3, the whole equation should be independent of f_t when all other parameters are held constant, and since the first term is quadratic in f_t and so are, too, the two arguments of $\phi_2(\cdot)$, it turns out that the function $\phi_2(\cdot)$ must be homogeneous of the first degree so that the factor f_t^2 in both members cancel out (this can also be proved by taking derivatives with respect to f_t and then invoking Euler's theorem for homogeneous functions). The final straightforward result is that the general equation for Δa_c meeting the required conditions is:

$$\Delta a_c = \frac{w_c^2 \ell_{ch}}{w_{ch}^2}\phi\left(\frac{w_c^2 \ell_{ch}}{w_{ch}^2 D}\right) \text{ or } \Delta a_c = \frac{w_c^2 E^\star}{G_f}\phi\left(\frac{w_c^2 E^\star}{G_f D}\right) \tag{7}$$

in which, obviously, $\phi(x) = \phi_2(1/x, 1)$.

The present result is consistent with the asymptotic results of Planas and Elices (1993) in which a lower bound for Δa_c was found for $D \to \infty$ which was, moreover, found to be very close to the actual asymptotic value. The lower bound $\Delta a_{c\infty}^*$ is given by:

$$\Delta a_{c\infty}^* = \frac{\pi}{32}\frac{w_c^2 E^\star}{G_f} \approx \lim_{D\to\infty} \Delta a_c. \tag{8}$$

Therefore, it is expected that $\phi(0) \approx \pi/32$.

Since Eq. (7) is numerically obtained, it is possible, just by cross-plotting the results, to solve it for w_c. The resulting equation takes the form:

[5] In the present case, i.e., for an orthotropic material (wood) considered in the configuration shown in Fig. 2, $E^\star = \{(2E_L E_T)/[(E_L/(2G_{LT}) - \nu_{LT} + (E_L/E_T)^{1/2}]\}^{1/2} = 696$ MPa.

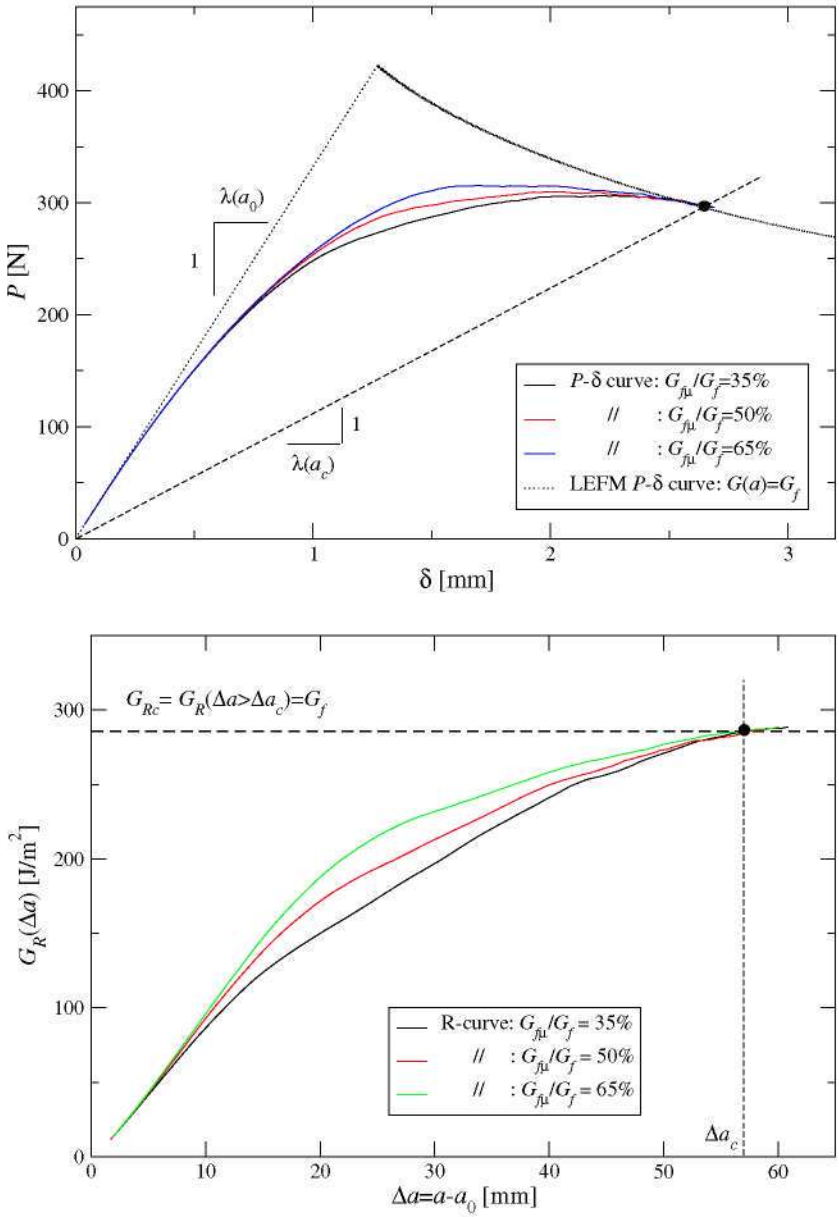

Fig. 9. Load–displacement curves (a) and their corresponding R-curves (b) obtained from DCB specimen in the case of different cohesive energy distributions corresponding to the ratios $G_{f\mu}/G_f = 35\%$, 50% and 65% while the cohesive fracture energy G_f, the tensile strength f_t and the critical opening w_c are kept constant ($G_f = 286\,\mathrm{J/m^2}$, $f_t = 1.0\,\mathrm{MPa}$ and $w_c = 1.0\,\mathrm{mm}$).

$$w_c = \sqrt{\frac{32\Delta a_c G_f}{\pi E^\star}}\psi\left(\frac{\Delta a_c}{D}\right) \tag{9}$$

The function $\psi(\cdot)$ is expected to aproach 1.0 as $D \to \infty$, i.e., $\psi(0) \approx 1$. The numerical results for $\psi(\cdot)$ have been plotted in Fig. 13.

On the other hand, various studies propose to experimentally measure w_c by mounting an extensometer in alignment with the initial notch tip (Lindhagen and Berglund, 2000; Sørensen, 2002; Sørensen and Jacobsen, 2003, 2009). However, another estimate of the critical opening is possible which avoids an experimental measure. Indeed, within the framework of 'equivalent LEFM' (based on FE computation performed on a purely elastic material), an approximation of w_c can be obtained from the *compliance* function $\varpi(a)$ which is estimated from the ratio of the crack opening in alignment with the initial notch tip (i.e., for the crack length a_0) over the applied load P. Thus, knowing the crack length a_c corresponding to the onset of the plateau value G_{Rc} of the R-curve and the load P_c corresponding to this crack length a_c, the critical opening w_c can be approximated by $w_c \simeq P_c\,\varpi(a_c)$. As shown in the Table 1, 'equivalent LEFM' through the *compliance* function $\varpi(a)$ leads to fair approximation of the critical opening w_c (underestimation of around 10%) in the case of the DCB specimen. Note that similar results have been obtained for the other specimen geometries (TDCB and SENB).

4.2. Dependence of the initial part of the R-curve on f_t and size

The general form of the R-curve can be written in dimensionless form as an extension of Eq. (4):

$$\frac{\Delta a}{\ell_{ch}} = \ddot{\varsigma}_1\left(\frac{G_R}{G_f}, \frac{D}{\ell_{ch}}, \frac{w_c}{w_{ch}}, \frac{G_{f\mu}}{G_f}\right), \tag{10}$$

in which Δa is the crack extension corresponding to a resistance G_R and, for a given specimen and material, all the other arguments are constant.

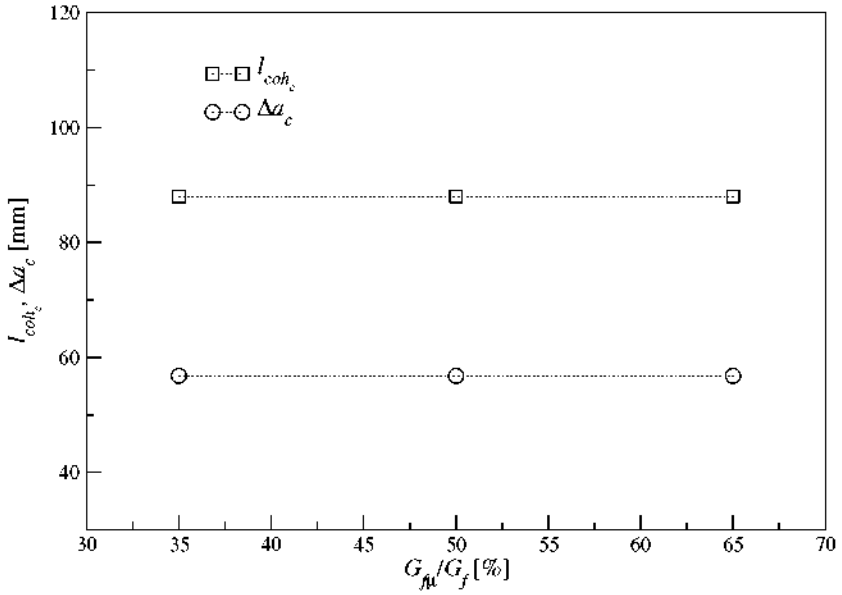

Fig. 10. Critical length of the cohesive zone l_{cohc} and its equivalent LEFM length $\Delta a_c = a_c - a_0$ with respect to the cohesive energy distributions $G_{f\mu}/G_f = 35\%$, 50% and 65%.

On the other hand, Fig. 7(b) shows that the initial part of the R-curve, say for $G_R \lesssim 0.25G_f$, the influence of w_c is very small and can be ignored in a first approximation. Similarly, Fig. 9(b) shows that the influence of $G_{f\mu}/G_f$ is also negligible over that range. Therefore, if we determine the effective crack extension $\Delta a_{0.2}$ that corresponds to a fixed ratio $G_R/G_f = 0.2 < 0.25$ as shown in Fig. 11(b), the result may be taken to be independent of w_c/w_{ch} and of $G_{f\mu}/G_f$ and so we have:

$$\frac{\Delta a_{0.2}}{\ell_{ch}} = \xi_1\left(0.2, \frac{D}{\ell_{ch}}, \frac{w_c}{w_{ch}}, \frac{G_{f\mu}}{G_f}\right) \approx \xi_1\left(0.2, \frac{D}{\ell_{ch}}\right) = \xi_2\left(\frac{D}{\ell_{ch}}\right). \tag{11}$$

Let us now divide both sides of the latter equation by D/ℓ_{ch} to get a relationship between $\Delta a_{0.2}/D$ and D/ℓ_{ch}, which can be rewritten as:

$$\frac{\ell_{ch}}{D} = \chi_1\left(\frac{D}{\Delta a_{0.2}}\right), \tag{12}$$

which can be solved for f_t in the form:

$$f_t = \sqrt{E^\star G_f/D}\,\chi\left(\frac{D}{\Delta a_{0.2}}\right), \tag{13}$$

where $\chi(\cdot)$ can be determined pointwise from the numerical results in Fig. 11b by finding Δa (i.e., $\Delta a_{0.2}$) for an ordinate $G_R = 0.2 \times 286 = 57.2\ \mathrm{J/m^2}$. Fig. 14 shows the results and a reasonable power law curve fit as:

$$f_t \approx 0.0916\sqrt{E^\star G_f/D}\left(\frac{D}{\Delta a_{0.2}}\right)^{2/3}. \tag{14}$$

4.3. Using R-curve analysis to determine the bilinear softening parameters

From the results of the previous sections, we see that the four parameters which characterize the bilinear softening curve influence the R-curve in ways much neater than their influences on the load–displacement curve. Therefore, the R-curve analysis, which is straightforward to carry out from experimental and numerical tests, can be used to determine the softening curve in a more efficient way than "blind fitting" procedures or than more optimized methods funded, for instance, on genetic algorithm (see Ref Dourado et al., 2008, for a recent study). A general procedure can be set as follows:

(1) Carry out stable load–displacement tests on DCB specimens (or TDCB, or SENB), and compute the experimental R-curves.
(2) On the experimental R-curve, localize the plateau and determine the resistance over it G_{Rc} and the equivalent LEFM crack extension at the initiation of the plateau, Δa_c. The cohesive fracture energy is then $G_f = G_{Rc}$ (Section 3.1).
(3) According to the result in Section 4.1, given G_f, $E^\star$, Δa_c and the specimen size D, w_c is determined from Eq. (9) which is to be obtained numerically for the specimen geometry from a curve as that in Fig. 13. Note that this curve can be determined for any (reasonable) values of f_t and $G_{f\mu}/G_f$.

    Alternatively, if the curve relative to Eq. (9) is not determined before hand, the critical opening w_c can be analytically estimated with a reasonable accuracy within the framework of 'equivalent LEFM' from the *compliance* function $\varpi(a)$ as $w_c \simeq P_c\varpi(a_c)$ where P_c is the external load corresponding to the equivalent crack length a_c. Note that such an analytical method avoids an experimental measure of the critical opening w_c.
    However, if a more accurate estimate of w_c is required, the solution can be iteratively obtained by changing the value of the critical crack opening w_c until the resulting Δa_c matches the experimental result within a reasonable accuracy. Such iteration will be well posed since, according to the results shown in Section 3.2, the critical crack extension Δa_c increases monotonically with w_c.

(4) Next, on the experimental R-curve, the extension $\Delta a_{0.2}$ for $G_R = 0.2G_f$ is determined, and, following the results in Section 4.2, the tensile strength f_t is determined from a numerically approximation of the relationship (13) such as that in Eq. (14), determined as shown in Fig. 14.

    Nevertheless, if such curve has not been determined before hand, the result can still be obtained by iterating over different values of f_t until the numerical result for $\Delta a_{0.2}$ matches the experimental result within a reasonable accuracy. In this

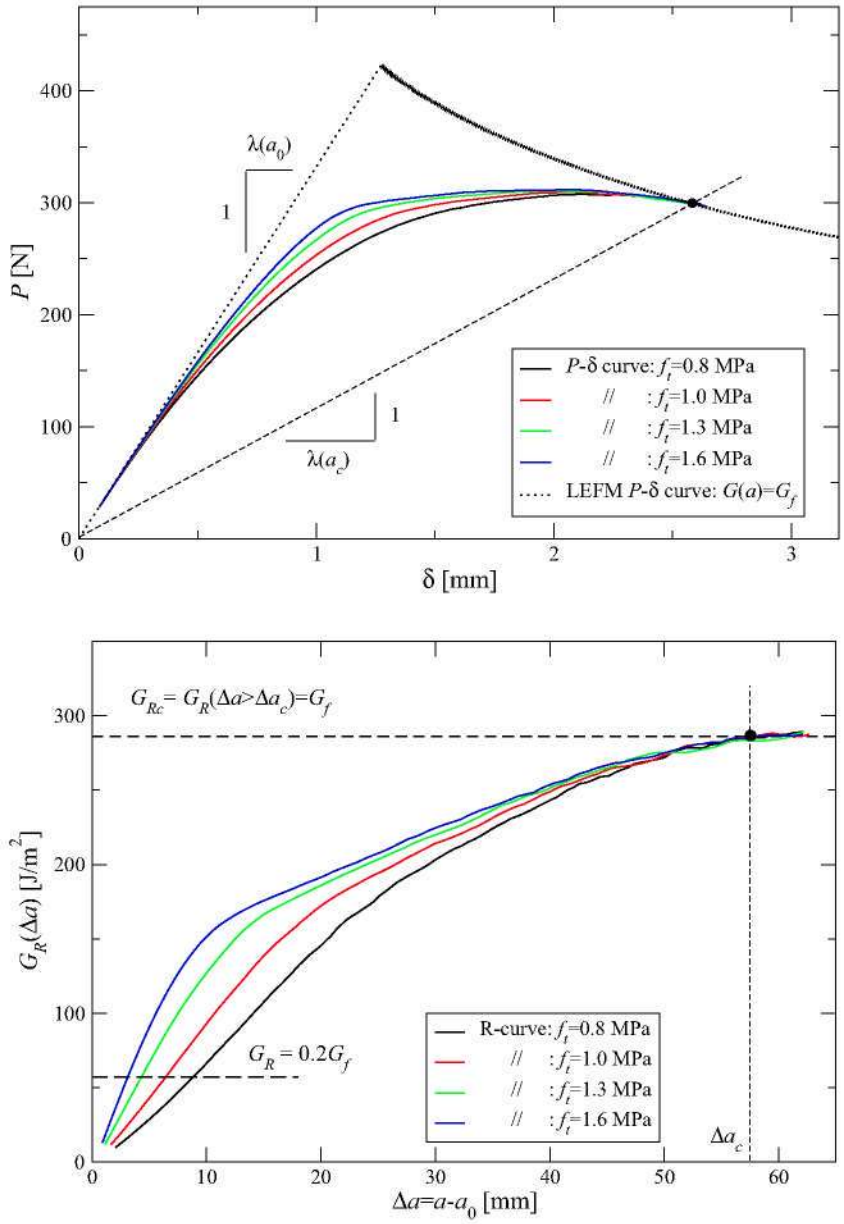

Fig. 11. Load–displacement curves (a) and their corresponding R-curves (b) obtained from the DCB specimen in the case of different tensile strength values f_t = 0.8, 1.0, 1.3 and 1.6 MPa while, the cohesive fracture energy G_f, the energy distribution and the critical opening w_c are kept constant (G_f = 286 J/m^2, $G_{f\mu}/G_f$ = 50% and w_c = 1.0 mm).

case, the dependency of $\Delta a_{0.2}$ on f_t is monotonically decreasing (as shown in Fig. 11b), but, according to the results in Fig. 14, the problem will again be well posed.

(5) Once the cohesive crack properties characterizing the plateau of the R-curve (i.e., G_f, w_c) and its initial part (i.e., f_t) have been determined, the only remaining parameter is the ratio of the cohesive energy distribution ($G_{f\mu}/G_f$). In this case, it is not possible to find a function of one variable to describe its influence since this parameter influences mainly the central portion of the R curve and the peak load, but is coupled to f_t and w_c. Therefore, direct iteration is advisable either to fit the value at a central point on the R-curve (or the peak load) or to use some optimization method for a weighted objective function, with weights concentrated on the middle half of the R-curve. Since this is a univariate optimization process, no special problems are envisaged.

Note that the order of the data reduction steps is crucial to get the cohesive properties. Indeed, the cohesive fracture energy G_f (estimated in step 2) is needed to obtained the critical opening w_c in step (3) and to get the tensile strength f_t in step (4), and, all three parameters are required to solve for $G_{f\mu}/G_f$ in step (5). Moreover, if steps (4) and (5) need numerical simulations with CZM, these steps are less time consuming than "blind fitting" procedures. Indeed, the more time consuming step corresponds to step (5) for which the simulations must be performed up to the peak load or to a central point of the R-curve (but this step does not need to reach the steady state of the cohesive zone) while, the tensile strength f_t in step (4) is estimated from the onset of the cohesive zone development (i.e., for small crack length increments Δa in terms of 'equivalent LEFM').

Finally, with the exception of the equality between the cohesive fracture energy G_f and the plateau value of the resistance G_{Rc} (Section 3.1), the connections established between the cohesive zone

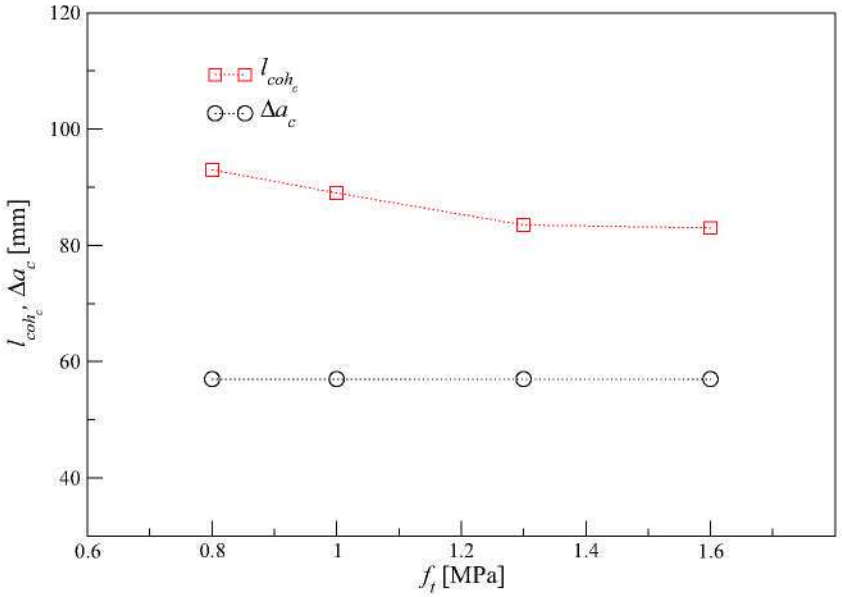

Fig. 12. Critical length of the cohesive zone l_{coh_c} and its equivalent LEFM length $\Delta a_c = a_c - a_0$ with respect to the tensile strength $f_t = 0.8,\ 1.0,\ 1.3$ and 1.6 MPa.

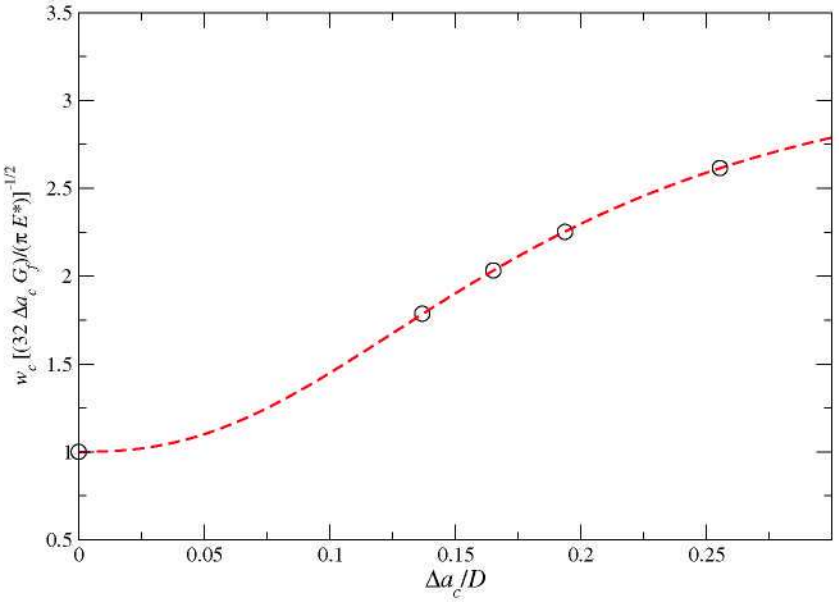

Fig. 13. Dimensionless relationship between the critical crack opening w_c, the critical equivalent crack extension Δa_c and the specimen size for the DCB specimen [Eq. (9)].

Table 1
Estimate of the critical opening w_c from equivalent LEFM : $w_c \simeq P_c \varpi(a_c)$. The values of w_c, Δa_c and P_c correspond to the numerical simulations plotted in Fig. 7.

w_c [mm]	Δa_c [mm]	P_c [N]	$\varpi(a_c)$ [10^{-3} mm/N]	$w_{ceq\,LEFM}$ [mm]
0.8	47.9	315	2.25	0.7 (13%)
1.0	57.8	300	2.89	0.9 (10%)
1.2	67.8	290	3.64	1.1 (9%)
1.6	89.4	265	5.62	1.5 (6%)

properties and the R-curve (detailed in Sections 3.2, 3.3 and 3.4) appear to be geometry and material dependent, as shown by Eqs. (9), (10) and (13). However, the results obtained for the other geometries (TDCB and SENB specimens) show that, although not identical, those connections follow a similar trend, and, thus, a procedure such as the one outlined here is applicable.

5. Conclusion

If the determination of the cohesive zone parameters based on experimental tests performed on DCB specimens loaded with pure bending moments is now well established and documented, such a method is not easily applicable for quasibrittle materials used in Civil Engineering because of the difficulty to apply a pure bending moment without inducing brittle failures and/or the consequent self-weight of specimens which turns difficult sophisticated loading setup. Nevertheless, the one-to-one correspondence which exists between the R-curve and the softening curve previously studied by Suo et al. (1992) is here revisited and adapted to quasi-brittle fracture (bilinear approximation of the concave softening) and to specimen loaded with forces.

The bilinear cohesive function is described from the cohesive fracture energy G_f, the critical opening w_c, a ratio characterizing

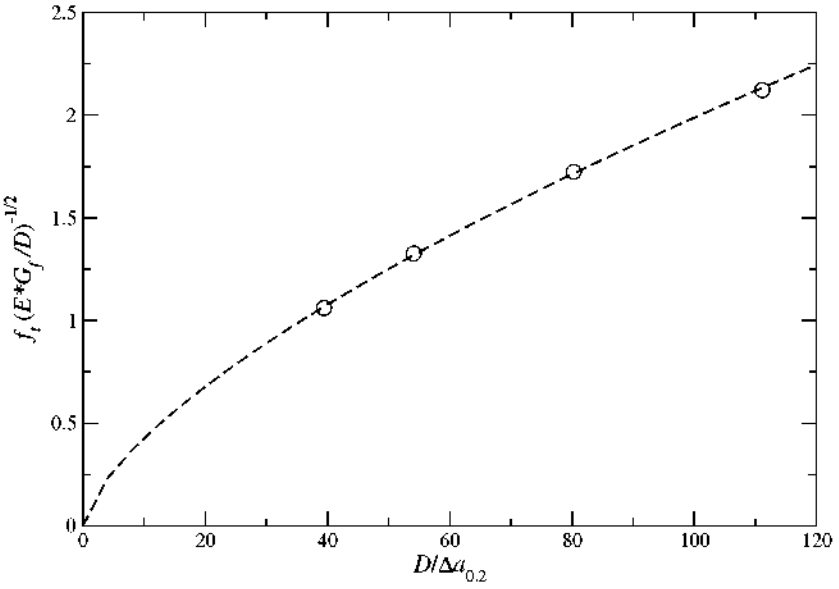

Fig. 14. Dimensionless representation of the tensile strength f_t as a function of $\Delta a_{0.2}$ [Eq. (14)].

the energy distribution with respect to the opening (noted as $G_{f\mu}/G_f$) and the tensile strength f_t.

From the observation of the well-known steady state regime of the cohesive zone which leads to the equality between the cohesive fracture energy G_f and the plateau value of the R-curve G_{Rc}, it has been shown that the cohesive parameters affect the load–displacement response and its corresponding 'equivalent LEFM' R-curve over nearly disjoint zones. The critical opening w_c has a dominant influence on the equivalent crack length increment Δa_c for which the plateau value of the R-curve occurs; the tensile strength f_t has a dominant influence over the initial part of the R-curve ($G_R \lesssim 0.25G_f$) while the energy distribution (given by the ratio $G_{f\mu}/G_f$) influences significantly the intermediate part of the load–displacement curve around the peak load and especially the maximum load itself as well as the middle half of the raising part of the R-curve (leaving unchanged both the starting part and the plateau).

Moreover, with the exception of the equality between the cohesive fracture energy G_f and the plateau value of the resistance G_{Rc}, even though the connections between the cohesive parameters and the R-curve are shown to be geometry and material dependent, their trends are preserved for the various geometries analyzed (DCB, TDCB and SENB).

Finally, the four parameters characterizing the bilinear softening are shown to influence the R-curve in ways much neater than their influences on the load–displacement curve. Therefore, the R-curve analysis, which is straightforward to carry out from experimental and numerical tests, can be used to determine the softening curve in a more efficient way than "blind fitting" procedures usually used in quasibrittle materials. On this basis, the outline of a general procedure is proposed which is applicable to any kind of specimen geometry and loading insofar as geometry and loading allow to achieve the steady state propagation. The application of the proposed procedure, funded on equivalent LEFM, requires only the load–displacement measurement of the tested specimen and presents the advantage to strongly limit the CZM simulations.

References

Bažant, Z.P., 2002. Concrete fracture models: testing and practice. Engineering Fracture Mechanics 69, 165–205.

Boström, L., 1994. The stress–displacement relation of wood perpendicular to the grain. Wood Science and Technology 28, 309–317.

Chandra, N., Li, H., Shet, C., Ghonem, H., 2002. Some issues in the application of cohesive zone models for metal-ceramics interfaces. International Journal of Solids and Structures 39, 2827–2855.

Coureau, J.-L., Morel, S., Gustafsson, P.J., Lespine, C., 2006. Influence of the fracture softening behaviour of wood on load–COD curves and R-curve. Materials and Structures 40, 97–106.

Dasgupta, R., Hay, J.C., Ortiz-Longo, C.R., White, K.W., Vipulanandan, C., 1998. Experimental study of the microstructural influence of the strain-softening behavior of cement mortar. Cement Concrete Research 28 (10), 1429–1444.

Dourado, N., Morel, S., de Moura, M.F.S.F., Valentin, G., Morais, J., 2008. Comparison of fracture properties of two wood species through cohesive crack simulations. Composites Part A: Applied Science and Manufacturing 39, 415–427.

Elices, M., Planas, 1993. The equivalent elastic crack: 1. Load-Y equivalences. International Journal of Fracture 61, 159–172.

Elices, M., Guinea, G.V., Gómez, J., Planas, J., 2002. The cohesive zone model: advantage, limitations and challenges. Eugineeriug Fracture Mechanics 69, 137–163.

Ferreira, L.E.T., Bittencourt, T.N., Sousa, J.L.A.O., Gettu, R., 2002. R-curve behavior in notched beam tests of rocks. Engineering Fracture Mechanics 69, 1845–1852.

Fett, T., Munz, D., Geraghty, R.D., White, K.W., 2000. Influence of specimen geometry and relative crack size on the R-curve. Engineering Fracture Mechanics 66, 375–386.

Guinea, G.V., 1995. Modelling the fracture of concrete: the cohesive crack. Materials and Structures 28, 187–194.

Hillerborg, A., Modeer, M., Petersson, P.E., 1976. Analysis of crack formation and crack growth in concrete by means of fracture mechanics and finite elements. Cement Concrete Research 06, 773–782.

Lespine, C.I., 2007. Influence de la géométrie des structures sur les propriétés de rupture dans les matériaux quasi-fragiles. Ph.D. thesis, US2B, Université Bordeaux 1, France, 2007 (Influence of the structure geometry on fracture properties in quasibrittle materials; in French).

Lindhagen, J.E., Berglund, L.A., 2000. Application of bridging-law concepts to short-fibre composites. Part 1: DCB test procedures for bridging law and fracture energy. Composites Science and Technology 60, 871–883.

Morel, S., Mourot, G., Schmittbuhl, J., 2003. Influence of the specimen geometry on R-curve behavior and roughnening of fracture surfaces. International Journal of Fracture 121, 23–42.

Morel, S., Dourado, N., Valentin, G., Morais, J., 2005. Wood: a quasibrittle material R-curve behavior and peak load evaluation. International Journal of Fracture 131, 385–400.

Park, K., Paulino, G.H., Roesler, J.R., 2008. Determination of the kink point in the bilinear softening model for concrete. Engineering Fracture Mechanics 75, 3806–3818.

Petersson, P.E., 1981. Crack growth and development of fracture zone in plain concrete and similar materials. Report TVBM-1006, Lund University, Sweden.

Planas, J., Elices, M., 1993. Asymptotic analysis of a cohesive crack: 2. Influence of the softening curve. International Journal of Fracture 64, 221–237.

Planas, J., Elices, M., Ruiz, G., 1993. The equivalent elastic crack: 2. X–Y equivalences and asymptotic analysis. International Journal of Fracture 61, 231–246.

Planas, J., Elices, M., Guinea, G.V., Gómez, F.J., Cendón, D.A., Arbilla, I., 2003. Generalizations and specializations of cohesive crack models. Engineering Fracture Mechanics 70, 1759–1776.

Sørensen, B.F., 2002. Cohesive law and notch sensitivity of adhesive joints. Acta Materialia 50, 1053–1061.
Sørensen, B.F., Jacobsen, T.K., 2003. Determination of cohesive laws by the J integral approach. Engineering Fracture Mechanics 70 (14), 1841–1858.
Sørensen, B.F., Jacobsen, T.K., 2009. Characterizing delamination of fibre composites by mixed mode cohesive laws. Composites Science and Technology 69, 445–456.
Suo, Z., Bao, G., Fan, B., 1992. Delamination R-curve phenomena due to damage. Journal of the Mechanics and Physics of Solids 40 (1), 1–16.
Wang, J., 2006. Cohesive zone model of intermediate crack-induced debonding of FRP-plated concrete beam. International Journal of Solids and Structures 43, 6630–6648.